Journal of Systems Engineering and Electronics
Vol. 32, No. 4, August 2021, pp.764 – 778

Polarization quaternion DOA estimation based on vector MISC array

SHAO Shuai[1], LIU Aijun[1,*], YU Changjun[1], and ZHAO Quanrui[2]

1. School of Electronics and Information Engineering, Harbin Institute of Technology, Harbin 150001, China;
2. Shanghai Radio Equipment Research Institute, Shanghai 201109, China

Abstract: This paper examines the direction of arrival (DOA) estimation for polarized signals impinging on a sparse vector sensor array which is based on the maximum interelement spacing constraint (MISC). The vector array effectively utilizes the polarization domain information of incident signals, and the quaternion model is adopted for signals polarization characteristic maintenance and computational burden reduction. The features of MISC arrays are crucial to the mutual coupling effects reduction and higher degrees of freedom (DOFs). The quaternion data model based on vector MISC arrays is established, which extends the scalar MISC array into the vector MISC array. Based on the model, a quaternion multiple signal classification (MUSIC) algorithm based on vector MISC arrays is proposed for DOA estimation. The algorithm combines the advantages of the quaternion model and the vector MISC array to enhance the DOA estimation performance. Analytical simulations are performed to certify the capability of the algorithm.

Keywords: direction of arrival (DOA), vector sensor array, vector maximum interelement spacing constraint (MISC) array, polarization quaternion model, quaternion multiple signal classification (Q-MUSIC).

DOI: 10.23919/JSEE.2021.000066

1. Introduction

Array signal processing is a basic theory in the fields of radar, sonar, navigation, etc [1,2]. With the increasing reliability of vector sensors, polarization is added to the direction of arrival (DOA) estimation as a basic information attribute. Therefore, many researchers proposed multi-component data processing algorithms. For polarization vector sensor arrays, multiple signal classification (MUSIC)-like algorithms were introduced in [3] and estimation of signal parameter via rotational invariance techniques (ESPRIT) were introduced in [4]. Nehorai et al. [5] studied the Cramer-Rao bound (CRB) for the vector-sensor arrays. In [6], a multiscale disambiguation algorithm based on a multiscale sparse array of spatially spread electromagnetic vector-sensor (SS-EMVS) array was developed to attain high accuracy and unambiguous DOA estimations. In [7], a joint estimation of DOA and polarization of the signals was attained based on SS-EMVS array, which can efficaciously decrease the complexity of the four-dimensional space joint estimation. Cao et al. [8] achieved the DOA estimation of correlated/coherent signals using a uniform rectangular array (URA) with electromagnetic vector-sensors. In [9], the proposed algorithm based on a sparse rectangular spatially spread crossed-dipole polarization sensitive array attained the two-dimensional (2D) DOA estimation which used the lowest components polarized vector sensor array and retained low mutual coupling. Song et al. [10] proposed a method which utilized the signals, inherent time-frequency peculiarity to obtain better performance of DOA estimation with a few snapshots for the underlying vector-sensor array in a noisy and coherent situation. In [11], Yang et al. proposed a hybrid L-shaped array of two sparse scalar arrays and a single triangular SS-EMVS for 2D DOA estimation, which obtained a better estimation performance. Ahmed et al. [12] proposed a fast quadrilinear decomposition algorithm for DOA and polarization estimation by an EMVS-URA, which kept rapid convergence and accurate parameter estimation. In [13], an estimation algorithm of 2D DOA and polarization parameter was proposed based on the three-parallel co-prime polarization sensitive array, which enhanced the estimation accuracy even in low signal-to-noise (SNR) ratio situation.

However, these methods presume that the complex valued data model represents incident signal frequency domain samples. The data covariance matrix is next described as second order statistical magnitude between all

Manuscript received January 29, 2021.
*Corresponding author.
This work was supported by the National Natural Science Foundation of China (62031015).

sensor components. In the recent few decades, algorithms based on quaternion were introduced [14] for array signal processing. A multidimensional complex signals hypercomplex version [15] was also introduced by Bülow et al. [16]. In [17], Miron et al. proposed a quaternion data model algorithm based on vector-sensor array for estimation of DOA and polarization parameters, which decreased the data covariance model representation memory size leading to an efficient algorithm. In [18], for L-shaped array, the dimension reduction Q-MUSIC algorithm was proposed to decrease the complexity. In [19], a generalized rotation invariance based quaternion multiple signal classification algorithm was proposed for the estimation of polarization parameters and DOA, which not only reduced the computation complexity considerably, but also avoided the performance degradation caused by the failure in parameters pairing. The DOA could be estimated by biquaternion MUSIC in [20] to achieve better angle measurement performance. A quaternion-based ESPRIT-type algorithm called augmented quaternion ESPRIT was proposed for DOA estimation with a co-located crossed-dipole array in [21] to achieve better performance in low SNR scenarios.

The main advantages of sensor arrays are their spatial selectivity and their ability to decrease interference and enhance signal quality. Traditional uniform linear arrays (ULAs) are commonly used sensor arrays, in which the spacing between elements does not exceed half wavelength and is constant to avert spatial aliasing. However, the traditional ULA degrees of freedom (DOFs) are merely linear to the sensor number. For a ULA of N sensors, the traditional subspace methods [22] may distinguish up to $N-1$ signals. For heightening the traditional ULA DOFs, additional sensors are needed, resulting in an extra complexity. Traditional ULAs also endure serious mutual coupling influence from array sensors. The sparse arrays, nonuniform linear arrays (NLAs), provide an interesting resolution for these difficulties. In sparse arrays, the mutual coupling influence can be decreased because of the interelement spacing increase [23]. Latterly, the sparse arrays advancement, for instance nested arrays [24] and coprime arrays (CAs) [25], have attracted researchers to review this subject because sparse arrays can be methodically devised and their DOFs can be analytically offered from closed-form formulas.

The nested array can provide $O(N^2)$ DOFs with merely N sensors, which is achieved via increasing interelement spacing and incorporating two or more ULAs [24]. The two-level nested array is composed of two ULAs. However, the nested array DOFs become lower than that of the minimum redundancy array for a given sensors number. Yang et al. [26] introduced an improved nested array (INA) by enlarging the outer ULA interelement spacing and adding an additional sensor. The INA offer higher DOFs and retain all the two-level nested array advantages. The CA is another interesting sparse array. The CA [25] includes two ULAs in which the first ULA is N'-sensor array with $\frac{N''\lambda}{2}$ interelement spacing, while the second ULA is N''-sensor array with $\frac{N'\lambda}{2}$ interelement spacing, where λ is signal wavelength and N' and N'' are coprime integers. For the nested array, the mutual coupling is further decreased in the CA. However, for the same number of physical sensors, the DOFs provided via a coprime array usually become smaller than that via a nested array. For further enlarging the DOFs, Pal et al. [27] proposed an extended CA via doubling the sensor number in an ULA. Its difference coarray may achieve consecutive lags between $(-N'N''-N''+1)$ and $(N'N''+N''-1)$ via using $(N'+N''-1)$ sensors. In [28], the CAs were derived from achieving two procedures. One procedure is constricting the subarray interelement spacing in the CA providing a compressed interelement spacing (CACIS). The CACIS normally enlarges the unique and consecutive lags number. To avoid a considerable number of overlaps of self-lags and cross-lags, in [28], the second procedure was proposed for displacing a subarray in the CA in order to offer a larger array aperture, a higher unique lags number, and a much larger minimum interelement spacing from the obtained CA with displaced subarrays. In [29], Zheng introduced an advanced array based on the maximum interelement spacing constraint (MISC) principle, which provided a higher DOFs and mutual coupling influence reduction.

At present, MISC arrays are only composed of scalar sensors and fail to display the polarization information of signals. The MISC array is composed of vector sensors, because it takes advantage of the array manifold, and takes into account the signal polarization information, which brings more benefits to DOA estimation. Based on the above analysis, this paper proposes a quaternion MUSIC based on vector MISC array.

This paper consists of the following sections. In Section 2, short quaternion descriptions are introduced and a polarized signal model is given. The MISC array concept is introduced and the characteristics of MISC array are discussed in Section 3. In Section 4, a description of the quaternion DOA estimation based on vector MISC array is given. In Section 5, the algorithm performances are evaluated by computer simulations. Finally, the conclu-

sions are presented in Section 6.

2. Quaternion data model of polarized signals

2.1 Polarization model

Quaternions discovered by Hamilton in 1843 are four-dimensional (4D) hypercomplex numbers, which are complex numbers extensions into 4D space. A quaternion is defined via one real and three imaginaries, whose Cartesian form can be described as

$$q = w + x\mathrm{i} + y\mathrm{j} + z\mathrm{k} \tag{1}$$

where $\mathrm{i}^2 = \mathrm{j}^2 = \mathrm{k}^2 = \mathrm{ijk} = -1$, $\mathrm{ij} = \mathrm{k}$, $\mathrm{ji} = -\mathrm{k}$, $\mathrm{ki} = \mathrm{j}$, $\mathrm{ik} = -\mathrm{j}$, $\mathrm{jk} = \mathrm{i}$, $\mathrm{kj} = -\mathrm{i}$.

Many books researched quaternions and their characteristics. The hypercomplex numbers basics were introduced in [30], while a comprehensive quaternions review was introduced in [31]. Several complex numbers properties may be extended into quaternions: the conjugate $q^* = w - x\mathrm{i} - y\mathrm{j} - z\mathrm{k}$; pure quaternion $q = x\mathrm{i} + y\mathrm{j} + z\mathrm{k}$; quaternion modulus $\|q\| = \sqrt{w^2 + x^2 + y^2 + z^2}$; quaternion inverse $q^{-1} = \dfrac{q^*}{\|q\|^2}$. The quaternions set, noted $\mathbb{H}$, forms a noncommutative normed algebra, meaning

$$q_1 q_2 \neq q_2 q_1. \tag{2}$$

And conjugation over $\mathbb{H}$ is an anti-involution

$$(q_1 q_2)^* = q_2^* \cdot q_1^*. \tag{3}$$

In [32], a Cayley-Dickson form quaternion was expressed as: $q = q_1 + q_2\mathrm{j}$, where $q_1 = w + x\mathrm{i}$ and $q_2 = y + z\mathrm{i}$. That is

$$q = \begin{bmatrix} 1 & \mathrm{j} \end{bmatrix} \begin{bmatrix} q_1 \\ q_2 \end{bmatrix}. \tag{4}$$

The joint expression of spatial domain and polarization domain of signals is modeled and the signal receiving model of electromagnetic vector sensor array is established. This paper mainly studies fully polarized electromagnetic waves.

Assuming that there is a point signal source with elevation angle θ and azimuth angle ϕ at a certain point in space. The ideal transmission medium is transmitted to the array along the direction of the Poynting vector, as shown in Fig. 1.

The unit vectors pointing in the positive direction of x, y, and z axis are denoted as $\boldsymbol{e}_x$, $\boldsymbol{e}_y$, and $\boldsymbol{e}_z$ respectively. The coordinate origin serves as the reference phase point of the electromagnetic vector sensor array, and the electromagnetic waves received are converted into baseband electrical signals.

As can be seen from Fig. 1, the unit vector of the incident direction of the signal is the propagation vector of the signal

$$\boldsymbol{e}_P = \begin{bmatrix} -\sin\theta\cos\phi & -\sin\theta\sin\phi & -\cos\theta \end{bmatrix}^{\mathrm{T}} \tag{5}$$

where the superscript T represents the transpose.

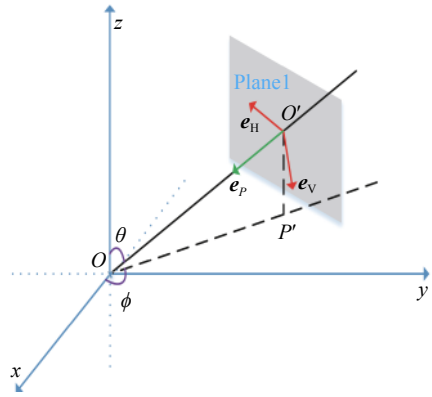

Fig. 1 Characterization of fully polarized electromagnetic waves

The horizontal vector $\boldsymbol{e}_{\mathrm{H}}$ and the vertical vector $\boldsymbol{e}_{\mathrm{V}}$ constitute a set of standard orthogonal basis perpendicular to the plane of the propagation direction:

$$\boldsymbol{e}_{\mathrm{H}} = \begin{bmatrix} -\sin\phi & \cos\phi & 0 \end{bmatrix}^{\mathrm{T}}, \tag{6}$$

$$\boldsymbol{e}_{\mathrm{V}} = \begin{bmatrix} \cos\theta\cos\phi & \cos\theta\sin\phi & -\sin\theta \end{bmatrix}^{\mathrm{T}}. \tag{7}$$

For the electromagnetic wave at point P in space, the complex analytical formula of the instantaneous electric field vector is

$$\boldsymbol{E} = E_{\mathrm{H}}(t)\boldsymbol{e}_{\mathrm{H}} + E_{\mathrm{V}}(t)\boldsymbol{e}_{\mathrm{V}} = [\boldsymbol{e}_{\mathrm{H}} \ \ \boldsymbol{e}_{\mathrm{V}}] \begin{bmatrix} E_{\mathrm{H}}(t) \\ E_{\mathrm{V}}(t) \end{bmatrix} \tag{8}$$

where

$$\begin{cases} E_{\mathrm{H}}(t) = E_{\mathrm{Hm}} \mathrm{e}^{\mathrm{i}(w_c t + \varphi_{\mathrm{H}})} \\ E_{\mathrm{V}}(t) = E_{\mathrm{Vm}} \mathrm{e}^{\mathrm{i}(w_c t + \varphi_{\mathrm{V}})} \end{cases}. \tag{9}$$

Equation (9) is the instantaneous projection of the complex analytical formula of the electric field vector in the horizontal and the vertical directions at time t. E_{Hm} and E_{Vm} are maximums in the horizontal and the vertical directions, respectively. The signal polarization information may be described via the instantaneous ratio of the electric field amplitude and phase in the vertical and the horizontal directions, and $\tan\gamma = \dfrac{E_{\mathrm{Vm}}}{E_{\mathrm{Hm}}}$, $\eta = \varphi_{\mathrm{V}} - \varphi_{\mathrm{H}}$, $\gamma \in \left[0, \dfrac{\pi}{2}\right]$ is polarization assist angle, and $\eta \in [0, 2\pi]$ is polarization phase difference. For a fully polarized wave, its endpoint polarization trajectory is an ellipse with a fixed long and short axial ratio and inclination. That is

$$\begin{bmatrix} E_{\mathrm{H}}(t) \\ E_{\mathrm{V}}(t) \end{bmatrix} = \frac{E_{\mathrm{H}}(t)}{\cos\gamma}\begin{bmatrix} \cos\gamma \\ \sin\gamma \mathrm{e}^{\mathrm{i}\eta} \end{bmatrix} = E_{\mathrm{c}}(t)\begin{bmatrix} \cos\gamma \\ \sin\gamma \mathrm{e}^{\mathrm{i}\eta} \end{bmatrix}. \tag{10}$$

The coordinates of the electric field vector in the plane rectangular coordinate system are

$$\begin{bmatrix} \boldsymbol{E}_x(t) \\ \boldsymbol{E}_y(t) \\ \boldsymbol{E}_z(t) \end{bmatrix} = \begin{bmatrix} \boldsymbol{e}_{\mathrm{H}} & \boldsymbol{e}_{\mathrm{V}} \end{bmatrix}\begin{bmatrix} \cos\gamma \\ \sin\gamma \mathrm{e}^{\mathrm{i}\eta} \end{bmatrix} E_{\mathrm{c}}(t). \tag{11}$$

The coordinates of the magnetic field in the plane rectangular coordinate system are

$$\begin{bmatrix} \boldsymbol{H}_x(t) \\ \boldsymbol{H}_y(t) \\ \boldsymbol{H}_z(t) \end{bmatrix} = \begin{bmatrix} \boldsymbol{e}_{\mathrm{V}} & -\boldsymbol{e}_{\mathrm{H}} \end{bmatrix}\begin{bmatrix} \cos\gamma \\ \sin\gamma \mathrm{e}^{\mathrm{i}\eta} \end{bmatrix} E_{\mathrm{c}}(t). \tag{12}$$

The coordinates of a complete six-dimensional electric and magnetic field in a plane rectangular coordinate system are

$$\begin{bmatrix} \boldsymbol{E}_x(t) \\ \boldsymbol{E}_y(t) \\ \boldsymbol{E}_z(t) \\ \boldsymbol{H}_x(t) \\ \boldsymbol{H}_y(t) \\ \boldsymbol{H}_z(t) \end{bmatrix} = \begin{bmatrix} -\sin\phi & \cos\theta\cos\phi \\ \cos\phi & \cos\theta\sin\phi \\ 0 & -\sin\theta \\ \cos\theta\cos\phi & \sin\phi \\ \cos\theta\sin\phi & -\cos\phi \\ -\sin\theta & 0 \end{bmatrix} \cdot \begin{bmatrix} \cos\gamma \\ \sin\gamma \mathrm{e}^{\mathrm{i}\eta} \end{bmatrix} E_{\mathrm{c}}(t) \tag{13}$$

where

$$\boldsymbol{A}_P(\phi,\theta,\gamma,\eta) = \boldsymbol{\beta}(\phi,\theta)\boldsymbol{P}(\gamma,\eta) = \begin{bmatrix} -\sin\phi & \cos\theta\cos\phi \\ \cos\phi & \cos\theta\sin\phi \\ 0 & -\sin\theta \\ \cos\theta\cos\phi & \sin\phi \\ \cos\theta\sin\phi & -\cos\phi \\ -\sin\theta & 0 \end{bmatrix} \begin{bmatrix} \cos\gamma \\ \sin\gamma \mathrm{e}^{\mathrm{i}\eta} \end{bmatrix}. \tag{14}$$

$\boldsymbol{A}_P(\phi,\theta,\gamma,\eta)$ is the polarization steering vector and $\boldsymbol{\beta}(\phi,\theta)$ shows the dependence of the polarization domain scan vector on the azimuth and elevation of the electromagnetic wave.

There is a uniform linear N electromagnetic vector sensor array along the positive direction of the y-axis. The electromagnetic vector sensor at the origin is used as the reference element. The electric dipoles of the electric field are orthogonal to each other, and the distance between the electromagnetic vector sensor array elements is d, and $d < \frac{\lambda}{2}$, which is used to ensure that there is no array blur, that is, the expected direction of the incident signal is only one value. When $\frac{\lambda}{2}$ is taken as the value, the array element utilization rate is the highest and the effect is guaranteed. λ is the wavelength of the incident desired signal. The y-axis coordinate y_n of the nth electromagnetic vector sensor is $(n-1)d$, $n = 1, 2, \cdots, N$, in Fig. 2. And make $M(M<N)$ far-field expected signals (fully polarized waves) incident on the array and the elevation angle $\theta = 90°$. For the azimuth of the desired signal, the spatial phase delay between the nth element and the reference element is

$$\alpha_n = -\frac{2\pi(n-1)d\sin\phi}{\lambda}, \tag{15}$$

and $d = \frac{\lambda}{2}$

$$\alpha_n = -\pi(n-1)\sin\phi. \tag{16}$$

The steering vector is

$$\boldsymbol{A}_s = \begin{bmatrix} \mathrm{e}^{\mathrm{i}\alpha_1} & \mathrm{e}^{\mathrm{i}\alpha_2} & \cdots & \mathrm{e}^{\mathrm{i}\alpha_N} \end{bmatrix}^{\mathrm{T}}. \tag{17}$$

The data received by the entire array is

$$\boldsymbol{X}(t) = \begin{bmatrix} \mathrm{e}^{\mathrm{i}\alpha_1}\boldsymbol{A}_P s(t) \\ \mathrm{e}^{\mathrm{i}\alpha_2}\boldsymbol{A}_P s(t) \\ \vdots \\ \mathrm{e}^{\mathrm{i}\alpha_N}\boldsymbol{A}_P s(t) \end{bmatrix} + \begin{bmatrix} \boldsymbol{n}_1(t) \\ \boldsymbol{n}_2(t) \\ \vdots \\ \boldsymbol{n}_N(t) \end{bmatrix} = \boldsymbol{A}_s(\phi,\theta)\otimes\boldsymbol{A}_P(\phi,\theta,\gamma,\eta)s(t) + \boldsymbol{N}(t) \tag{18}$$

where $\boldsymbol{n}_n(t) = [n_{ny}(t) \quad n_{nz}(t)]^{\mathrm{T}}, (n = 1, 2, \cdots, N)$ is the noise vector in directions of y and z. $\otimes$ represents the Kronecker product. It is assumed that the noise is independent between each array element, the noise is independent between the vector components within each array element, and the signal and noise are relatively independent. Noise is an independent Gaussian white noise with a zero mean and a σ^2 variance.

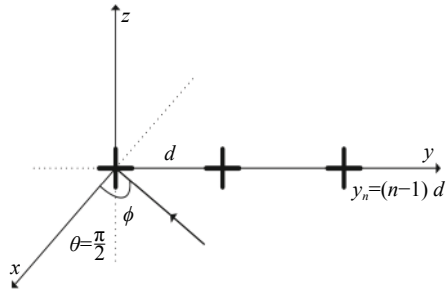

Fig. 2 Uniform linear array

2.2 Quaternions data model

Take the Y and Z direction electric field components in (14) to obtain the polarization domain steering vector of the m th signal received by this electromagnetic vector sensor array

$$\boldsymbol{A}_P(\phi_m,\theta_m,\gamma_m,\eta_m)=\left[\begin{array}{cc}\cos\phi_m & \cos\theta_m\sin\phi_m\\ 0 & -\sin\theta_m\end{array}\right]\left[\begin{array}{c}\cos\gamma_m\\ \sin\gamma_m\mathrm{e}^{\mathrm{i}\eta_m}\end{array}\right]. \tag{19}$$

The elevation $\theta=90°$, and after simplification

$$\boldsymbol{A}_P(\phi_m,\gamma_m,\eta_m)=\left[\begin{array}{c}\cos\phi_m\cos\gamma_m\\ -\sin\gamma_m\mathrm{e}^{\mathrm{i}\eta_m}\end{array}\right]. \tag{20}$$

Apply (4) here. The quaternion Cayley-Dickson representation synthesizes the polarization domain steering vector in the complex number domain into a polarization domain steering parameter in the quaternion domain, namely

$$p(\phi_m,\gamma_m,\eta_m)=\left[\begin{array}{cc}1 & \mathrm{j}\end{array}\right]\left[\begin{array}{c}\cos\phi_m\cos\gamma_m\\ -\sin\gamma_m\mathrm{e}^{\mathrm{i}\eta_m}\end{array}\right]. \tag{21}$$

After simplification, (21) becomes

$$p=\cos\phi_m\cos\gamma_m-\sin\gamma_m\cos\eta_m\mathrm{j}-\sin\gamma_m\sin\eta_m\mathrm{k}. \tag{22}$$

According to (18), it can be known that the mth signal received by the entire electromagnetic vector sensor array is

$$\boldsymbol{X}_m(t)=\boldsymbol{A}_s(\phi_m)\,p(\phi_m,\gamma_m,\eta_m)\,s_m(t)+\boldsymbol{N}(t) \tag{23}$$

where

$$\boldsymbol{A}_s(\phi_m)=\left[\begin{array}{cccc}\mathrm{e}^{\mathrm{i}\alpha_{m,1}} & \mathrm{e}^{\mathrm{i}\alpha_{m,2}} & \cdots & \mathrm{e}^{\mathrm{i}\alpha_{m,N}}\end{array}\right]^{\mathrm{T}}. \tag{24}$$

The quaternion noise is synthesized from the complex noise vector by Cayley-Dickson representation as

$$n_n=\left[\begin{array}{cc}1 & \mathrm{j}\end{array}\right]\left[\begin{array}{c}n_{ny}(t)\\ n_{nz}(t)\end{array}\right]=n_{ny}+n_{nz}\mathrm{j}. \tag{25}$$

All signals received by the entire array can be expressed as

$$\boldsymbol{X}(t)=\sum_{m=1}^{M}\boldsymbol{A}_s(\phi_m)\,p(\phi_m,\gamma_m,\eta_m)\,s_m(t)+\boldsymbol{N}(t) \tag{26}$$

where

$$\boldsymbol{N}(t)=\left[\begin{array}{cccc}n_1 & n_2 & \cdots & n_N\end{array}\right]^{\mathrm{T}}. \tag{27}$$

Make $\boldsymbol{a}_m=\boldsymbol{A}_s(\phi_m)\,p(\phi_m,\gamma_m,\eta_m)$, and write (26) as a matrix

$$\boldsymbol{X}(t)=\left[\begin{array}{cccc}\boldsymbol{A}_{s1} & \boldsymbol{A}_{s2} & \cdots & \boldsymbol{A}_{sM}\end{array}\right]_{N\times M}\cdot\left[\begin{array}{cccc}p_1 & & & \\ & p_2 & & \\ & & \ddots & \\ & & & p_M\end{array}\right]_{M\times M}\left[\begin{array}{c}s_1(t)\\ s_2(t)\\ \vdots\\ s_M(t)\end{array}\right]_{M\times 1}=\boldsymbol{A}\boldsymbol{S}(t)+\boldsymbol{N}(t). \tag{28}$$

$\boldsymbol{A}$ is called the spatial-polarization joint steering vector matrix. In this way, a signal receiving data model of the electromagnetic vector sensor array in the quaternion domain is established.

3. MISC array

3.1 Difference coarray

Sensor positions of an N-sensor nonuniform linear array are given by $n_{\mathrm{num}}d$, in which n_{num} belongs to an integer set $S=\{n_{\mathrm{num}},\ \mathrm{num}=1,2,\cdots,N\}$ and $d=\dfrac{\lambda}{2}$ denotes the minimum distance between sensors. According to (24), the mth signal array steering vector is

$$\boldsymbol{A}_s(\phi_m)=\left[\begin{array}{cccc}\mathrm{e}^{\mathrm{i}\xi_{m,n_1}} & \mathrm{e}^{\mathrm{i}\xi_{m,n_2}} & \cdots & \mathrm{e}^{\mathrm{i}\xi_{m,n_N}}\end{array}\right]^{\mathrm{T}} \tag{29}$$

where

$$\xi_{m,n_{\mathrm{num}}}=-\frac{2\pi n_{\mathrm{num}}d\sin\phi_m}{\lambda}. \tag{30}$$

The data model is still (28), but the steering vector is (29). The covariance matrix of $\boldsymbol{X}(t)$ may be given by

$$\boldsymbol{R}_{XX}=\mathrm{E}\{\boldsymbol{X}(t)\boldsymbol{X}^{\triangleleft}(t)\}=\boldsymbol{A}\boldsymbol{R}_{SS}\boldsymbol{A}^{\triangleleft}+\mathrm{E}\{\boldsymbol{N}(t)\boldsymbol{N}^{\triangleleft}(t)\}=\sum_{m=1}^{M}\sigma_m^2\|p_m\|^2\boldsymbol{A}_{sm}\boldsymbol{A}_{sm}^{\triangleleft}+2\sigma^2\boldsymbol{I}_N \tag{31}$$

where $\mathrm{E}\{\cdot\}$ is the statistical expectation operator,

$$\boldsymbol{R}_{SS}=\mathrm{E}\{\boldsymbol{S}(t)\boldsymbol{S}^{\triangleleft}(t)\}=\mathrm{diag}\left(\left[\sigma_1^2\|p_1\|^2,\cdots,\sigma_M^2\|p_M\|^2\right]\right) \tag{32}$$

is the source covariance matrix, the superscripts $\triangleleft$ represents the quaternion conjugate transpose, diag(a) represents a diagonal matrix whose diagonal elements are a, $\boldsymbol{I}_N$ denotes the $N\times N$ identity matrix.

Vectorizing $\boldsymbol{R}_{XX}$ yields

$$\boldsymbol{z}=\mathrm{vec}(\boldsymbol{R}_{XX})=\mathrm{vec}\left(\sum_{m=1}^{M}\sigma_m^2\|p_m\|^2\boldsymbol{A}_{sm}\boldsymbol{A}_{sm}^{\triangleleft}\right)+2\sigma^2\boldsymbol{1}=\boldsymbol{B}\boldsymbol{p}+2\sigma^2\boldsymbol{1} \tag{33}$$

where vec($\cdot$) represents the vectorization operator by stacking all columns of a matrix into a column vector one by one, $\boldsymbol{B}=[\boldsymbol{b}(\phi_1),\cdots,\boldsymbol{b}(\phi_M)]$, $\boldsymbol{b}(\phi_m)=\boldsymbol{A}_{sm}^{*}\otimes\boldsymbol{A}_{sm}$, $\boldsymbol{p}=[\sigma_1^2,\cdots,\sigma_M^2]^{\mathrm{T}}$, and $\boldsymbol{1}=\mathrm{vec}(\boldsymbol{I}_N)=[\boldsymbol{1}_1^{\mathrm{T}},\cdots,\boldsymbol{1}_N^{\mathrm{T}}]^{\mathrm{T}}$ with $\boldsymbol{1}_m$ being a column zeros vector except a 1 at the mth position. By comparing (28) with (33), the vector $\boldsymbol{z}$ can be regarded as the data received from the coherent source signal vector $\boldsymbol{p}$ with a single snapshot, and $2\sigma^2\boldsymbol{1}$ becomes a deterministic noise term. The different rows of $\boldsymbol{B}$ behave

similarly to the manifold of a virtual array with expanded aperture, and the positions of its sensors are given by a set of differences D in Definition 1. This virtual array is known as the original array difference coarray [33]. Assuming that $U=[-L_u,L_u]$ is the D consecutive segment, the corresponding measurements can be rearranged as

$$\boldsymbol{z}_U=\boldsymbol{J}\boldsymbol{z}=\boldsymbol{B}'\boldsymbol{p}+2\sigma^2\boldsymbol{I}' \tag{34}$$

where L_u is the maximum of consecntive segment, $\boldsymbol{J}$ represents a $(2L_u+1)\times N^2$ selection matrix, $\boldsymbol{B}'$ is a $(2L_u+1)\times M$ consecutive virtual ULA U manifold matrix, and $\mathbf{1}'$ is a $(2L_u+1)\times 1$ zeros vector except a 1 at the (L_u+1)th position. The steering vector of the original matrix is shown in (24), and that of the virtual array is

$$\boldsymbol{A}_{\text{svir}}(\phi_m)=\left[\begin{array}{ccccc}1 & \mathrm{e}^{\mathrm{i}\frac{2\pi d\sin\phi_m}{\lambda}} & \mathrm{e}^{\mathrm{i}\frac{2\pi 2d\sin\phi_m}{\lambda}} & \cdots & \mathrm{e}^{\mathrm{i}\frac{2\pi L_u d\sin\phi_m}{\lambda}}\end{array}\right]^{\mathrm{T}}. \tag{35}$$

Definition 1 For a sensor position set $\boldsymbol{S}$ sparse array, its difference coarray D is defined as

$$D=\{n_1-n_2|n_1,n_2\in S\}. \tag{36}$$

Definition 2 [34] A sparse array S degrees of freedom is the difference coarray D cardinality.

Definition 3 [34] For a sparse array S, let U represent the difference coarray D maximum consecutive segment. The U cardinality is referred to as S uniform DOFs.

3.2 Mutual coupling

The received signal in (28) does not consider the sensor mutual coupling. However, in practice, the small separation mutual coupling effect cannot be neglected. After considering the mutual coupling effect, (28) can be viewed as

$$\boldsymbol{X}(t)=\boldsymbol{C}\boldsymbol{A}\boldsymbol{S}(t)+\boldsymbol{N}(t) \tag{37}$$

where $\boldsymbol{C}$ represents an $N\times N$ mutual coupling matrix.

The $\boldsymbol{C}$ expression is rather complicated. [35]. In ULA, $\boldsymbol{C}$ can be approximated by a B-banded symmetric Toeplitz matrix [36] as

$$\langle\boldsymbol{C}\rangle_{n_1,n_2}=\begin{cases}c_{|n_1-n_2|}, & |n_1-n_2|\leqslant B\\ 0, & \text{otherwise}\end{cases} \tag{38}$$

where $\langle\cdot\rangle_{n_1,n_2}$ denotes the (n_1, n_2)th matrix element, n_1, $n_2\in S$ and c_0, c_1,$\cdots$, c_B are coupling coefficients satisfying c_0=1>$|c_1|$>$|c_2|$>$\cdots$>$|c_B|$. The coupling coefficients magnitudes are inversely proportional to their sensor separations, $|c_g/c_l|=l/g$ for g, $l>0$ [36]. For the mutual coupling effect evaluation, the weight function and coupling leakage are usually employed.

Definition 4 An array S weight function $w(l)$ is defined as the sensor pair number that leads to coarray index l.

$$w(l)=\left|\left\{(n_1,n_2)\in S^2|n_1-n_2=l\right\}\right| \tag{39}$$

The weight function $w(l)$ for any linear array with N sensors [35] satisfies

$$w(0)=N,\sum_{l\in D}w(l)=N^2,w(l)=w(-l). \tag{40}$$

Definition 5 For a sensor number, the coupling leakage [35] is defined as the energy ratio:

$$CL=\frac{\left\|\boldsymbol{C}-\text{diag}(\boldsymbol{C})\right\|_{\text{F}}}{\|\boldsymbol{C}\|_{\text{F}}} \tag{41}$$

where $\left\|\boldsymbol{C}-\text{diag}(\boldsymbol{C})\right\|_{\text{F}}$ is all the off-diagonal components energy, characterizing the mutual coupling level, and $\|\cdot\|_{\text{F}}$ represents the Frobenius norm. A small value CL indicates the less significant mutual coupling.

3.3 Array structure

In this subsection, MISC array based on maximum interelement spacing constraint will be introduced. These arrays have many advantages. First, their sensor locations and the DOFs can be expressed in a closed form. In addition, the MISC arrays difference coarrays are hole-free. Most importantly, MISC arrays possess less mutual coupling effect and a higher DOF.

For an arbitrary sensor number, the MISC arrays are constructed by the given interelement spacings. Denote the maximum interelement spacing as D, and the associated interelement spacing set as A. Specifically, MISC arrays D and A are defined as

$$D=2\left\lfloor\frac{N}{4}\right\rfloor+2,\quad N\geqslant 5, \tag{42}$$

$$A_{\text{MISC}}=\{1,D-3,\underbrace{D,\cdots,D}_{N-D},\underbrace{2,\cdots,2}_{\frac{D-4}{2}},3,\underbrace{2,\cdots,2}_{\frac{D-4}{2}}\}, \tag{43}$$

where $\lfloor\cdot\rfloor$ denotes the integral part of the rational number in the square brackets.

The MISC array minimum sensor number is 5, $N\geqslant 5$. D increases as N increases.

The MISC array sensor position set is

$$\begin{aligned}S_{\text{MISC}}=\{&0,1,D-2,2D-2,\cdots,(N-D+1)D-2,\\&(N-D+1)D,\cdots,(N-D+2)D-6,(N-D+2)D-3,\\&(N-D+2)D-1,\cdots,(N-D+3)D-7\}.\end{aligned} \tag{44}$$

The MISC array sensor locations are shown in Fig. 3. Since D is decided by N, for an arbitrary sensor, MISC arrays have sensor positions closed-form expressions.

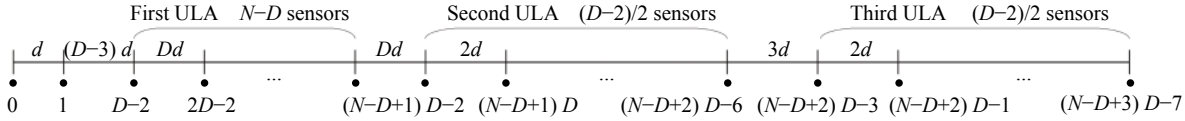

Fig. 3 MISC array configuration

3.4 Array analysis

In this subsection, we analyze the performance of MISC array and compare them with some other arrays. It is mainly analyzed from two aspects, which are DOFs and weight functions. The coprime arrays DOFs are calculated instead of uniform DOFs.

(i) Uniform DOFs

For the integer set S_{MISC}, the MISC array difference set is provided by $(N-D+3)D+7$ and $(N-D+3)D-7$ consecutive set

$$D_{\text{MISC}} = \{-(N-D+3)D+7, \cdots, -2, -1, 0, 1, 2, \cdots, (N-D+3)D-7\}. \tag{45}$$

The uniform DOFs of the MISC array is

$$\text{uDOFs}_{\text{MISC}} = 2(N-D+3)D-13. \tag{46}$$

Substituting D in (46) with (42) yields

$$\text{uDOFs}_{\text{MISC}} = 4N\left\lfloor\frac{N}{4}\right\rfloor - 8\left\lfloor\frac{N}{4}\right\rfloor^2 + 4N - 4\left\lfloor\frac{N}{4}\right\rfloor - 9. \tag{47}$$

For uniform DOFs, MISC arrays have closed-form expressions. Using $\frac{N}{4}$ instead of $\left\lfloor\frac{N}{4}\right\rfloor$, (47) can be approximately expressed as

$$\text{uDOFs}_{\text{MISC}} \approx \frac{N^2}{2} + 3N - 9 \tag{48}$$

where the approximation does not alter the magnitude orders.

For comparison, the DOFs of arrays, such as ULA, CA, and INA are described below. For ULA, the uniform DOFs are calculated. The ULA uniform DOFs array is

$$\text{uDOFs}_{\text{ULA}} = 2N-1. \tag{49}$$

For the coprime array, the zeroth position element can be shared, so there are $(N'+N''-1)$ elements

$$\text{uDOFs}_{\text{CA}} \approx N'N'', \quad N'+N''=N. \tag{50}$$

The INA provides hole-free difference coarrays [26]. This indicates that the MISC array is sparser and has a larger array aperture than the improved nested array, thus it is much less sensitive to mutual coupling effects. The uniform DOFs for the improved nested arrays are given by

$$\text{uDOFs}_{\text{INA}} = \begin{cases} \frac{N^2}{2} + 2N - \frac{7}{2}, & N \text{ is odd} \\ \frac{N^2}{2} + 2N - 3, & N \text{ is even} \end{cases}. \tag{51}$$

From (48), the MISC array uniform DOFs has the N^2 magnitude order. Therefore, the MISC array has a higher uniform DOFs than the INA. At the same time, the DOFs of MISC array is higher than that of the coprime array, and much higher than that of the ULA.

(ii) Weight function

MISC array's another advantage is less mutual coupling. For mutual coupling effects, the weight functions at small separations are more important [37]. The first three weight functions, $w(1)$, $w(2)$, and $w(3)$, provide a major influence on the mutual coupling, and $w(1)$ has the greatest influence [34].

According to the interelement spacing set A_{MISC} and the weight function definition, its weight functions $w(1)$, $w(2)$, and $w(3)$ are

$$w(1)=1, w(2)=2\left\lfloor\frac{N}{4}\right\rfloor-2, \quad w(3)=\begin{cases} 1, & N\neq 8,9,10,11 \\ 2, & N=8,9,10,11 \end{cases}. \tag{52}$$

In comparison, the first three weight functions for ULA are

$$w(1)=N-1, w(2)=N-2, w(3)=N-3, \tag{53}$$

and those for the coprime array are

$$w(1)=w(2)=w(3)=2. \tag{54}$$

For improved nested arrays, D and A are calculated when N is small, that is

$$\begin{cases} N=2, D=2, A=\{1\} \\ N=3, D=3, A=\{1,2\} \\ N=4, D=3, A=\{1,3,2\} \\ N=5, D=4, A=\{1,1,4,3\} \\ N=6, D=4, A=\{1,1,4,4,3\} \\ N=7, D=5, A=\{1,1,1,5,5,4\} \\ N=8, D=5, A=\{1,1,1,5,5,5,4\} \end{cases}. \tag{55}$$

For INAs, the first three weight functions are

$$w(1)=\begin{cases} 1, & N=2 \\ \frac{N+1}{2}-1, & N \text{ is odd; } N\geqslant 3 \\ \frac{N}{2}-1, & N \text{ is even; } N\geqslant 4 \end{cases}, \tag{56}$$

$$w(2)=\begin{cases} 1, & N=3,4 \\ 0, & \text{otherwise} \end{cases}, \tag{57}$$

$$w(3)=\begin{cases}1, & N=4,5,6\\ 0, & \text{otherwise}\end{cases}. \tag{58}$$

Through $w(1)$, $w(2)$, and $w(3)$, the mutual coupling effects of the MISC array is compared with two other sparse arrays. Although the coprime array provides a smaller $w(2)$ value, there are holes in the difference coarray. The MISC array is sparser than the improved nested array from the weight functions, so that the mutual coupling is greatly reduced.

4. Quaternion based DOA estimator

4.1 Quaternion spectral matrix

The spectral matrix [38] is proved by second order auto-moments and cross-moments of all antenna sensors for scalar-sensor arrays. For vector-sensor array, quaternion spectral matrix (QSM), which is the equivalent second order representation, $\boldsymbol{\Omega}\in\mathbb{H}^{N\times N}$ is

$$\boldsymbol{\Omega}=\mathrm{E}\{\boldsymbol{X}\boldsymbol{X}^{q}\} \tag{59}$$

where $\boldsymbol{X}\in\mathbb{H}^{N}$ is the quaternion observation vector from (28). Replacing (28) in (59) and using (3), $\boldsymbol{\Omega}$ can be expressed as

$$\begin{aligned}\boldsymbol{\Omega}&=\mathrm{E}\{(\boldsymbol{A}\boldsymbol{S}+\boldsymbol{N})(\boldsymbol{A}\boldsymbol{S}+\boldsymbol{N})^{q}\}=\\ &\mathrm{E}\{(\boldsymbol{A}\boldsymbol{S}+\boldsymbol{N})(\boldsymbol{S}^{q}\boldsymbol{A}^{q}+\boldsymbol{N}^{q})\}.\end{aligned} \tag{60}$$

Assume that the decorrelation between sources themselves and between the noise and the sources, and the quaternion spectral matrix is

$$\boldsymbol{\Omega}=\mathrm{E}\{\boldsymbol{A}\boldsymbol{S}\boldsymbol{S}^{q}\boldsymbol{A}^{q}\}+\mathrm{E}\{\boldsymbol{N}\boldsymbol{N}^{q}\}=\boldsymbol{\Omega}_{S}+\boldsymbol{\Omega}_{N} \tag{61}$$

where

$$\begin{aligned}\boldsymbol{\Omega}_{S}&=\boldsymbol{A}\mathrm{E}\{\boldsymbol{S}\boldsymbol{S}^{q}\}\boldsymbol{A}^{q}=\sum_{m=1}^{M}\sigma_{m}^{2}\boldsymbol{A}\boldsymbol{A}^{q}=\\ &\sum_{m=1}^{M}\sigma_{m}^{2}\|p_{m}\|^{2}\boldsymbol{A}_{sm}\boldsymbol{A}_{sm}^{q},\end{aligned} \tag{62}$$

and $\boldsymbol{\Omega}_{N}=\mathrm{E}\{\boldsymbol{N}\boldsymbol{N}^{q}\}$ is a matrix containing noise second order statistics. In (61), $\boldsymbol{\Omega}_{S}$ is the signal part and $\sigma_{m}^{2}\|p_{m}\|^{2}$ is the mth source power.

The vector sensor array $\boldsymbol{X}\in\mathbb{H}^{N}$ output can be expressed because of the complex-valued outputs $\boldsymbol{X}_{1},\boldsymbol{X}_{2}\in\mathbb{C}^{N}$ of the two components as

$$\boldsymbol{X}=\boldsymbol{X}_{1}+\boldsymbol{X}_{2}\mathrm{j}. \tag{63}$$

The quaternion vector transpose-conjugate $\boldsymbol{X}$ can be described by complex vectors transpose-conjugates $\boldsymbol{X}_{1}$, $\boldsymbol{X}_{2}$ as

$$\boldsymbol{X}^{q}=\boldsymbol{X}_{1}^{\mathrm{H}}-\mathrm{j}\boldsymbol{X}_{2}^{\mathrm{H}} \tag{64}$$

where the superscript H represents the conjugate transpose. Introduce (63) and (64) into (59), $\boldsymbol{\Omega}$ is

$$\begin{aligned}\boldsymbol{\Omega}&=\mathrm{E}\left\{(\boldsymbol{X}_{1}+\boldsymbol{X}_{2}\mathrm{j})\left(\boldsymbol{X}_{1}^{\mathrm{H}}-\mathrm{j}\boldsymbol{X}_{2}^{\mathrm{H}}\right)\right\}=\\ &\mathrm{E}\left\{\boldsymbol{X}_{1}\boldsymbol{X}_{1}^{\mathrm{H}}\right\}-\mathrm{E}\left\{\boldsymbol{X}_{1}\mathrm{j}\boldsymbol{X}_{2}^{\mathrm{H}}\right\}+\mathrm{E}\left\{\boldsymbol{X}_{2}\mathrm{j}\boldsymbol{X}_{1}^{\mathrm{H}}\right\}+\mathrm{E}\left\{\boldsymbol{X}_{2}\boldsymbol{X}_{2}^{\mathrm{H}}\right\}.\end{aligned} \tag{65}$$

In (65), $\boldsymbol{X}_{1}$, $\boldsymbol{X}_{2}$ are i-complex vectors and j and i multiplication is not commutative. In (65), for the two vector array components, auto-covariance and cross-covariance matrices mean that QSM contains all the second-order information intrinsically. The QSM noise-free part becomes a Toeplitz matrix [17]. Assuming the data (see (28)) noise component is spatially nonpolarized and white, the noise part is a real diagonal matrix and the diagonal entries indicate the N sensors noise power.

4.2 Subspace method

(i) Quaternion vector orthogonality

The received polarization components data of the electromagnetic vector sensor arrays are arranged in order and combined into a long vector data in the complex domain. The advantage of this is that the data can be placed in the complex domain and the complex algebra can be used for operations. However, the polarization components vector structure is destroyed because the data model in the complex domain does not take into account the orthogonality between the polarization components and just stacks the data into a long vector. The data is synthesized into a quaternion and the inherent orthogonality can accurately describe orthogonality between the received components in the quaternion domain instead of simply stacking up the data in the complex domain.

It can be seen that modeling in the quaternion domain can describe the polarization information more completely and accurately than modeling in the complex domain. The quaternion orthogonality has a stronger constraint than the complex one [17]. Theoretically quaternion orthogonality or long vector orthogonality are identical only if sources have identical polarizations or if there is only one source. Otherwise, these two methods obtain different results. Compared to the long vector method, the quaternion vector orthogonality to estimate the signal subspace improves estimation accuracy. The signals energy can be more precisely concentrated on a quaternion vector orthogonal basis than on a long vector one.

(ii) Quaternion eigenvalue decomposition

Eigen-structure methods are based on the vector space decomposition using energy criteria in orthogonal subspaces. Researchers in areas such as quantum mechanics [39], vector-signal processing [40], and color image processing [41] pay attention to singular value decomposi-

tion and eigenvalue decomposition (EVD) of quaternion matrices. In this paper, the quaternion eigenvalues and eigenvectors are utilized for right eigenvalues and eigenvectors. The quaternion spectral matrix $\hat{\boldsymbol{\Omega}}$ estimation is proved by statistical average

$$\hat{\boldsymbol{\Omega}} = \frac{1}{T}\sum_{sam=1}^{T} \boldsymbol{X}_{sam}\boldsymbol{X}_{sam}^{\mathbf{q}} \tag{66}$$

where T is the total of snapshots, $\boldsymbol{X}_{sam}$ is receiving array data at each snapshot and sam is the snapshot index. QSM becomes quaternion Hermitian $\hat{\boldsymbol{\Omega}}^{\mathbf{q}} = \hat{\boldsymbol{\Omega}}$ by construction. Quaternion Hermitian matrix eigenvalues are real-valued [42]. Quaternion spectral matrix becomes

$$\hat{\boldsymbol{\Omega}} = \sum_{n=1}^{N} \lambda_n \boldsymbol{u}_n \boldsymbol{u}_n^{\mathbf{q}} \tag{67}$$

where λ_n represents the real eigenvalue and $\boldsymbol{u}_n$ represents the N orthonormal quaternion eigenvector.

By recognition of (61) with (67), the first M eigenvalues correspond to the signal part and the rest N–M correspond to the noise part. And M is a priori known. The QSM can be expressed as

$$\boldsymbol{\Omega} = \boldsymbol{A}\boldsymbol{\Sigma}\boldsymbol{A}^{\mathbf{q}} + \boldsymbol{\Omega}_N \tag{68}$$

with $\boldsymbol{A} \in \boldsymbol{H}^{N\times M}$ including the M source vectors and $\boldsymbol{\Sigma} \in \mathbf{R}^{M\times M}$ a diagonal matrix including the sources powers. Assuming that noise is not polarized, its covariance matrix is diagonal and real: $\boldsymbol{\Omega}_N = 2\sigma^2\boldsymbol{I}_N$, where $2\sigma^2$ is the noise power. The $\boldsymbol{\Omega}$ EVD is

$$\boldsymbol{\Omega} = \boldsymbol{U}\boldsymbol{D}\boldsymbol{U}^{\mathbf{q}} \tag{69}$$

with $\boldsymbol{U} = [\boldsymbol{u}_1, \cdots, \boldsymbol{u}_N] \in \boldsymbol{H}^{N\times N}$ including the quaternion-valued N eigenvectors of $\boldsymbol{\Omega}$ and $\boldsymbol{D} \in \mathbf{R}^{\mathbf{N}\times\mathbf{N}}$, the eigenvalues diagonal matrix.

(iii) Quaternion MUSIC

Define two matrices $\boldsymbol{U}_S \in \boldsymbol{H}^{N\times M}$ and $\boldsymbol{U}_G \in \boldsymbol{H}^{N\times(N-M)}$ as

$$\boldsymbol{U}_S = [\boldsymbol{u}_1, \cdots, \boldsymbol{u}_M], \tag{70}$$

$$\boldsymbol{U}_G = [\boldsymbol{u}_{M+1}, \cdots, \boldsymbol{u}_N]. \tag{71}$$

$\boldsymbol{U}_S$ includes the signal subspace eigenvectors and $\boldsymbol{U}_G$ includes the noise subspace eigenvectors. By multiplying (68) on the right, we get

$$\boldsymbol{\Omega}\boldsymbol{U}_G = \boldsymbol{A}\boldsymbol{\Sigma}\boldsymbol{A}^{\mathbf{q}}\boldsymbol{U}_G + 2\sigma^2\boldsymbol{U}_G. \tag{72}$$

QSM can also be indicated according to $\boldsymbol{U}_S$ and $\boldsymbol{U}_G$ as

$$\boldsymbol{\Omega} = \boldsymbol{U}_S\boldsymbol{D}_S\boldsymbol{U}_S^{\mathbf{q}} + 2\sigma^2\boldsymbol{U}_G\boldsymbol{U}_G^{\mathbf{q}} \tag{73}$$

where $\boldsymbol{D}_S = \mathrm{diag}\{\lambda_1, \cdots, \lambda_M\}$. The noise power is equal for all array sensors, therefore the last N–M eigenvalues are $2\sigma^2$. Replace (73) in (72), and use the vectors orthogonality between $\boldsymbol{U}_S$ and $\boldsymbol{U}_G$, and the relation is obtained

$$2\sigma^2\boldsymbol{U}_G = \boldsymbol{A}\boldsymbol{\Sigma}\boldsymbol{A}^{\mathbf{q}}\boldsymbol{U}_G + 2\sigma^2\boldsymbol{U}_G \tag{74}$$

which implies

$$\boldsymbol{A}^{\mathbf{q}}\boldsymbol{U}_G = 0. \tag{75}$$

If (75) is multiplied on the right by $(\boldsymbol{A}^{\mathbf{q}}\boldsymbol{U}_G)^{\mathbf{q}}$, (75) can be expressed using columns of $\boldsymbol{A}$ as

$$\boldsymbol{a}_m^{\mathbf{q}}\boldsymbol{U}_G\boldsymbol{U}_G^{\mathbf{q}}\boldsymbol{a}_m = 0 \tag{76}$$

for all $\{\phi_m, \theta_m, \gamma_m, \eta_m\}$ sets corresponding to M signal sources parameters. $\boldsymbol{\Pi}_N = \boldsymbol{U}_G\boldsymbol{U}_G^{\mathbf{q}} \in \boldsymbol{H}^{N\times N}$ is the noise subspace projector. In reality, this projector estimation, $\hat{\boldsymbol{\Pi}}_N$, results from the estimated spectral matrix $\hat{\boldsymbol{\Omega}}$ EVD.

The quaternion DOA estimation based on vector MISC array is then calculated via projecting the quaternion steering vector $\boldsymbol{a}_m(\phi_m, \theta_m, \gamma_m, \eta_m) \in \boldsymbol{H}^N$,

$$\boldsymbol{a}_m = \begin{bmatrix} \mathrm{e}^{\mathrm{i}\xi_{m,n_1}} \\ \mathrm{e}^{\mathrm{i}\xi_{m,n_2}} \\ \vdots \\ \mathrm{e}^{\mathrm{i}\xi_{m,n_N}} \end{bmatrix} p(\phi_m, \theta_m, \gamma_m, \eta_m) \tag{77}$$

where $\xi_{m,n_{num}}$ is (30), on the noise subspace as

$$SP_{\mathrm{Q}}(\phi_m, \theta_m, \gamma_m, \eta_m) = \frac{1}{\boldsymbol{a}_m^{\mathbf{q}}\hat{\boldsymbol{\Pi}}_N\boldsymbol{a}_m}. \tag{78}$$

A quaternion estimation is similar to the scalar MUSIC algorithm. Equation (78) has maxima for $\{\phi_m, \theta_m, \gamma_m, \eta_m\}$ sets corresponding to signal sources. Varying φ_m, θ_m, γ_m, η_m, a 4D hypersurface is calculated. The ϕ_m, θ_m, γ_m, η_m estimation values are the maxima coordinates on this hypersurface. The first M maxima correspond to the M signal sources. The ϕ_m, θ_m, γ_m, η_m estimation process is quasi-unsupervised. In this paper, the DOA estimation of the signal is mainly concerned and the polarization of the signal is known. For the model described above, the elevation angle is 90°, and only the azimuth angle needs to be estimated.

4.3 Computational complexity

For long vectors and quaternion algorithms, this subsection addresses the computational complexity, only focusing on the covariance matrix estimation. As it indicates repetitive operations, this procedure best indicates the two algorithms' complexity difference. The method complexity is evaluated regarding memory traffic, memory requirements, and basic arithmetical operations: real numbers addition (A), multiplication (M) and division (D).

Consider a two-component vector sensor array $\boldsymbol{e}_y$ and $\boldsymbol{e}_z$. A snapshot is proved by two complex vectors $\boldsymbol{X}_1, \boldsymbol{X}_2 \in \mathbb{C}^N$. The observation quaternion form $\boldsymbol{X} \in \mathbb{H}^N$ has the expression proved by (63) and the long vector representation $\tilde{\boldsymbol{X}} \in \mathbb{C}^{2N}$ is

$$\tilde{\boldsymbol{X}} = \begin{bmatrix} \boldsymbol{X}_1 \\ \boldsymbol{X}_2 \end{bmatrix}. \tag{79}$$

The corresponding covariance matrices are

$$\boldsymbol{\Omega} = \mathrm{E}\{\boldsymbol{X}\boldsymbol{X}^{\mathrm{q}}\} \in \mathbb{H}^{N\times N}, \tag{80}$$

$$\tilde{\boldsymbol{\Omega}} = \mathrm{E}\left\{\tilde{\boldsymbol{X}}\tilde{\boldsymbol{X}}^{\mathrm{H}}\right\} \in \mathbb{C}^{2N\times 2N}. \tag{81}$$

Averaging over T the covariance matrix is used for estimation:

$$\boldsymbol{\Omega} = \frac{1}{T}\sum_{sam=1}^{T} \boldsymbol{X}_{sam}\boldsymbol{X}_{sam}^{\mathrm{q}} = \frac{1}{T}\sum_{sam=1}^{T} \boldsymbol{\Omega}_{sam}, \tag{82}$$

$$\tilde{\boldsymbol{\Omega}} = \frac{1}{T}\sum_{sam=1}^{T} \tilde{\boldsymbol{X}}_{sam}\tilde{\boldsymbol{X}}_{sam}^{\mathrm{H}} = \frac{1}{T}\sum_{sam=1}^{T} \tilde{\boldsymbol{\Omega}}_{sam}. \tag{83}$$

Each $\boldsymbol{\Omega}_{sam}$ matrices include N^2 quaternion entries and can be expressed for $4N^2$ real fields machine memory, while the $\tilde{\boldsymbol{\Omega}}_{sam}$ matrices have complex entries, corresponding to $8N^2$ real values. For the data covariance model, the quaternion algorithm reduces by half the memory requirements, resulting in memory traffic operations diminution by $\frac{1}{2}$ approximately and a proportional speed gain.

Evaluate the basic arithmetical operations number for covariance matrix estimation. Each quaternion entries of $\boldsymbol{\Omega}_{sam}$ is a result of two quaternions multiplication. It implies 16 real (M) and 12 real (A), and the total number of operations of the whole matrix are $16N^2$ (M) and $12N^2$ (A). $16N^2$ (M) and $8N^2$ (A) are calculated for the complex matrix $\tilde{\boldsymbol{\Omega}}_{sam}$. Thus, the summation $\boldsymbol{\Omega}$ have a total of $16N^2T$ (M) and $16N^2T-4N^2$ (A) while $\tilde{\boldsymbol{\Omega}}$ requires $16N^2T$ (M) and $16N^2T-8N^2$ (A). The division by T means $4N^2$ real numbers (D) for quaternions and $8N^2$ (D) for long vectors.

Regarding the real values elementary operations number, the quaternion model needs $4N^2$ (A) and $4N^2$ (D) less than the long vector model. The division computational complexity is several times more important than addition, meaning higher computational cost for long vectors.

The quaternion eigenvectors computation of the estimated matrix $\boldsymbol{\Omega} \in \boldsymbol{H}^{N\times N}$ can be executed by complex numbers or quaternions. The complex numbers methods diagonalize the $\boldsymbol{\Omega}$ complex adjoint matrix, a $2N\times 2N$ complex-valued matrix [43]. In [44], working in quaternion domain enhances the algorithms convergence speed compared to the complex method. This heightens the idea that the quaternions can enhance the algorithms' performance. The quaternion algorithms reduce computational efforts because of compact data handling.

5. Simulation results

In this section, numerical examples imply the superiority of the vector arrays based on quaternion over the scale arrays in terms of weight functions, mutual coupling matrices, and DOA estimation performance. Assume that the source number is known. For evaluating the results, the DOA root mean square error (RMSE) is defined as a 100 independent trials average:

$$\mathrm{RMSE} = \sqrt{\frac{1}{100M}\sum_{i=1}^{100}\sum_{m=1}^{M}\left(\hat{\bar{\phi}}^{(i)} - \bar{\phi}\right)^2} \tag{84}$$

where $\hat{\bar{\phi}}^{(i)}$ is the ith trial $\bar{\phi}$ estimate.

5.1 Weight functions and mutual coupling matrices

In the simulation example, the weight functions and mutual coupling matrices of the MISC array [29], the ULA [22], the CA [25], and the INA [24] are compared. For all these arrays, we consider that the number of sensors is 11. For the coprime array, the parameters are $N' = 5$ and $N'' = 7$. Here, the mutual coupling model (38) is described by $c_1 = 0.05\mathrm{e}^{\mathrm{i}\pi/3}$, B=100, and $c_l = c_1\mathrm{e}^{-\mathrm{i}(l-1)\pi/8}/l$ for $2 \leqslant l \leqslant B$. Fig. 4 indicates the weight functions of four kinds of arrays.

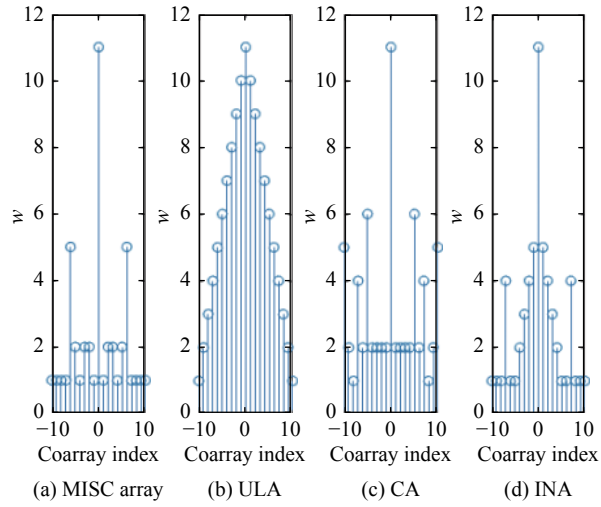

Fig. 4 Weight functions

In Fig. 4, the ULA has the largest weight functions ($w(1) = 10$, $w(2) = 9$, $w(3) = 8$). The improved nested array exhibits larger weight functions ($w(1) = 5$, $w(2) = 4$, $w(3) = 3$), due to the dense inner ULA. The coprime array provides smaller weight functions ($w(1) = w(2) = w(3) = 2$) because of sparser configuration. The weight functions ($w(1) = 1$, $w(2) = 2$, $w(3) = 2$) are even smaller for the MISC array.

Fig. 5 indicates the mutual coupling matrices magnitudes. The blue color indicates less energy. The nested array suffers from the severest mutual coupling effect. The MISC array and CA suffer from less mutual coupling effect.

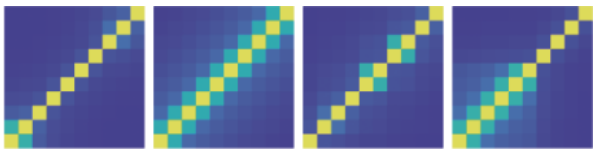

(a) MISC array (b) ULA (c) CA (d) INA

Fig. 5 Mutual coupling matrices

5.2 DOA estimation in the absence of mutual coupling

In the simulation example, in the absence of mutual coupling, the DOA estimation performance is compared among the MISC array, the ULA, the CA, and the INA. For all arrays, sensors number is 11. The MUSIC search interval is 0.01° and the incident angle is 30°. The phase difference of the polarization signal is 0 and the constant mode ratio is 0.5. The simulations analyze the RMSE performance about the input SNR, and the snapshots number respectively. The fixed parameter setting is $T = 1\,024$ snapshots. Fig. 6 displays the DOA estimation RMSE versus the input SNR.

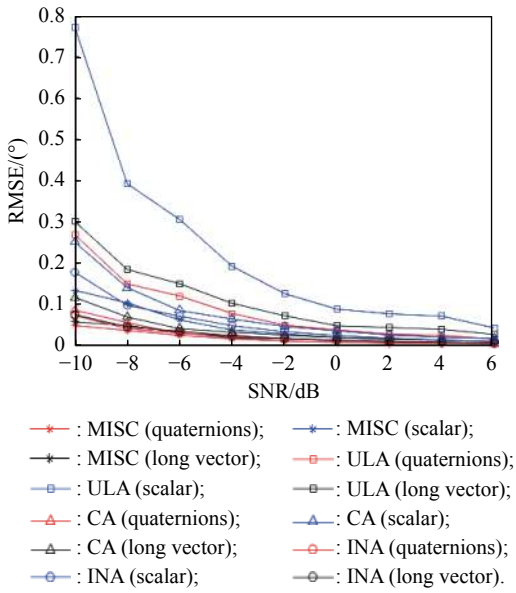

Fig. 6 RMSE of normalized DOA estimates versus the SNR without mutual coupling

All the RMSEs decrease as the SNR increases. When the SNR is higher than −4 dB, RMSEs attain a steady level. Moreover, the RMSE of the MISC array is smaller than that of the other arrays especially based on the quaternion algorithm.

Fig. 7 displays the DOA estimation RMSE about the snapshots number. All DOA estimations are more stabilized and accurate as the snapshots number increases, and the MISC array is better than other arrays. The overall quaternion-based algorithm is better than similar algorithms no matter how many snapshots are observed.

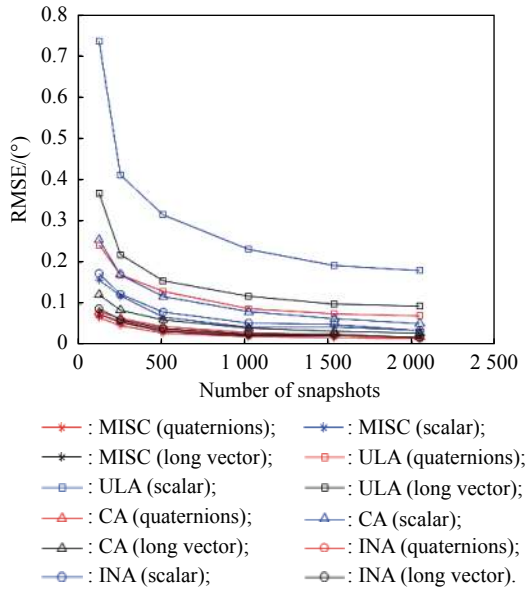

Fig. 7 RMSE of normalized DOA estimates versus the number of snapshots without mutual coupling

5.3 DOA estimation with mutual coupling

In the simulation, in the presence of mutual coupling, DOA estimation performance of the MISC array, the ULA, the CA, and the INA are compared. The sensors number is 11 and the incident angle is 30°. The RMSE performance about the input SNR, the snapshot number, and the coupling coefficient c_1 are analyzed. The DOA estimation RMSE about the SNR is displayed in Fig. 8. The quaternion algorithm for vector arrays exhibits better performance than for scale arrays. The three arrays outperform the ULA against mutual coupling effect.

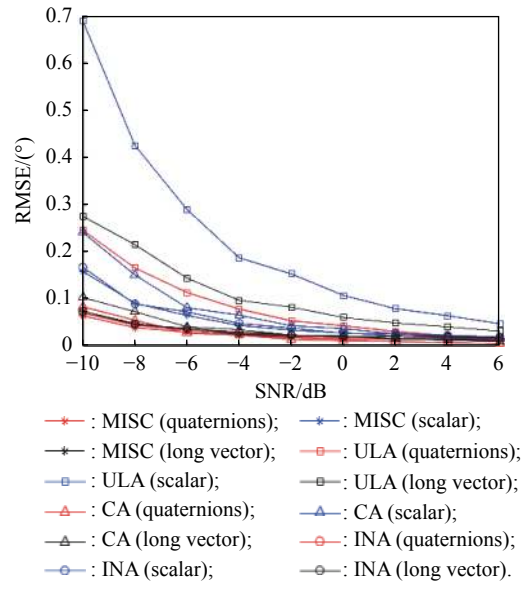

Fig. 8 RMSE of normalized DOA estimates versus the SNR with mutual coupling

In Fig. 9, the DOA estimation RMSE about the snapshots number is displayed. The RMSE is reduced rapidly for the arrays, as the snapshots number increases. For the quaternion algorithm, the RMSE results are reduced rather stably. The RMSE about $|c_1|$ is displayed in Fig. 10. Along with the $|c_1|$ increase, the RMSE increases for any array. More severe mutual coupling effect is introduced by a higher value of $|c_1|$. The CA has a better performance when $|c_1|$ is larger than 0.1.

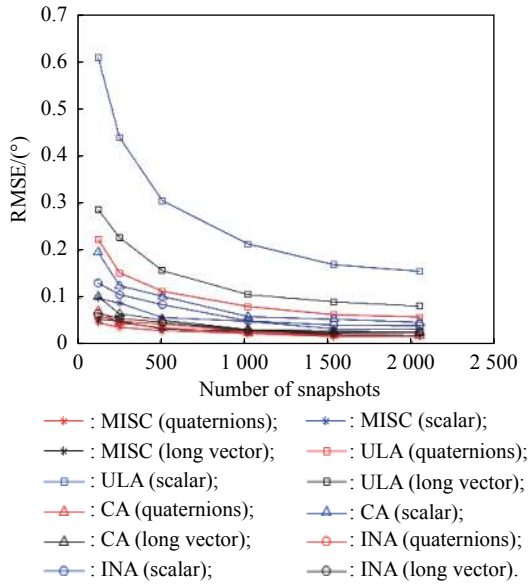

Fig. 9 RMSE of normalized DOA estimates versus the number of snapshots with mutual coupling

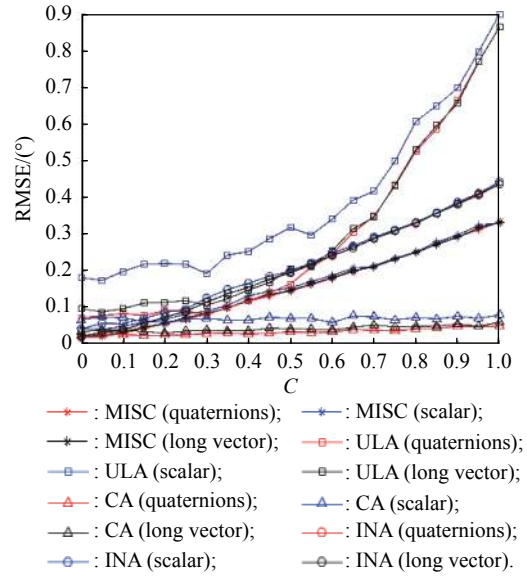

Fig. 10 RMSE of normalized DOA estimates versus the *c* with mutual coupling

5.4 Other aspects of simulation analysis

(i) CRB of the designed method

The CRB of the design method is analyzed. In order to highlight the design approach, it is taken out separately, and the approach is very close to its CRB. See Fig. 11 for details.

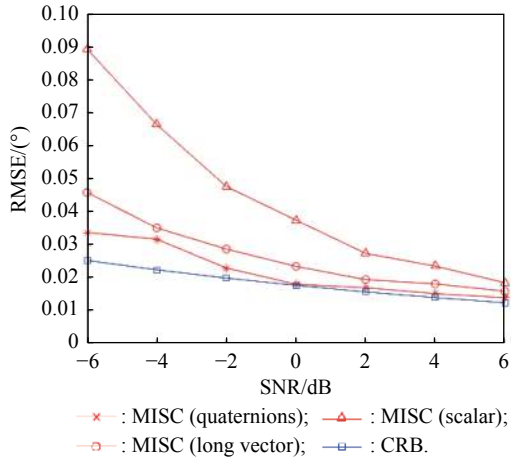

Fig. 11 CRB of the designed method

(ii) Influence of the minimum scan interval

The effect of the minimum scan interval is simulated and analyzed, as shown in Fig. 12. The simulation parameters are the same as before, using three scanning intervals, which are 0.01°, 0.05°, and 0.1° respectively. The incident angle is 30°. The smaller the interval, the more accurate the estimation, but the search time will also be longer. Therefore, keep scan intervals as small as possible, as computer power permits. Since the angle corresponding to the maximum value is directly selected as the estimate value in the search process, the quantization error is about half of the interval.

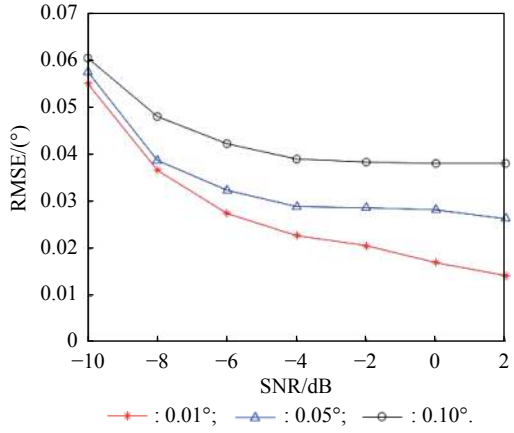

Fig. 12 Influence of minimum scan interval for designed method

(iii) Relationship between the probability of success and the SNR

In this section, the incident angle is 30°. DOA is estimated successfully if RMSEs are less than 0.05. Simulation parameters are the same as before, and a 0.01 inter-

val is used. The simulation results are shown in Fig. 13. As the SNR increases, the probability of success increases, and the quaternion algorithm has a better performance.

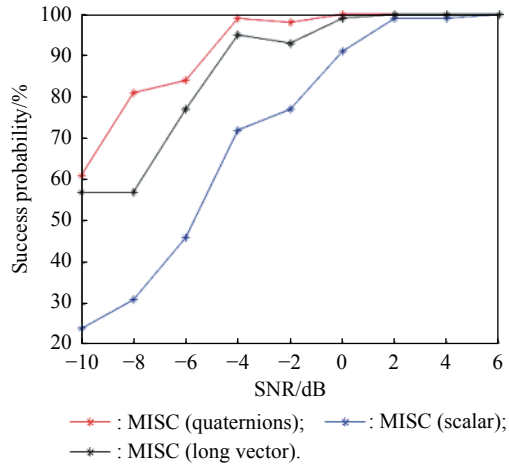

Fig. 13 Relationship between the probability of success and the SNR

(iv) Direction finding ability of the designed method for coherent sources

The performance of the algorithm in the case of coherent sources is analyzed by simulation. The incident angles of the two sources are 40° and 60° respectively. These two sources are coherent sources with the same signal form but slightly different polarization modes. As can be seen from the spectrum in Fig. 14, this method can distinguish sources but traditional methods cannot. It can be seen that the quaternion-based algorithm designed in this paper has a better performance.

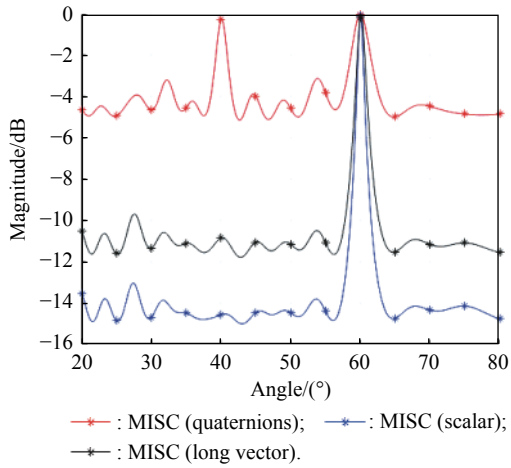

Fig. 14 Spectrum

6. Conclusions

In this paper, the combination of vector sensor array and quaternion algorithm shows advantages: higher DOFs, mutual coupling effect reduction, signals polarization characteristic maintenance, and computational burden reduction. For a given sensors number, the DOFs and the sensor locations in MISC array are uniquely determined and can be described via closed-form expressions. The quaternion data model based on vector arrays is established, which extends the scalar array into vector array. Based on the model, a quaternion MUSIC algorithm based on vector MISC arrays is proposed for DOA estimation. The algorithm combines the advantages of the quaternion model and the vector array to enhance the DOA estimation performance. The quaternion model has a lower RMSE. Coprime arrays also have good results under mutual coupling conditions. Analytical simulations are operated to certify the capability of the algorithm. Overall, the vector MISC array based on quaternion has a good effect.

References

[1] KRIM H, VIBERG M. Two decades of array signal processing research: the parametric approach. IEEE Signal Processing Magazine, 1996, 13(4): 67–94.
[2] TREES H L V. Optimum array processing: part IV of detection, estimation, and modulation theory. New Jersey: John Wiley & Sons, 2004.
[3] WONG K T, ZOLTOWSKI M D. Self-initiating music-based direction finding and polarization estimation in spatio-polarizational beamspace. IEEE Trans. on Antennas & Propagation, 2000, 48(8): 1235–1245.
[4] ZOLTOWSKI M D, WONG K T. Esprit-based 2-d direction finding with a sparse uniform array of electromagnetic vector sensors. IEEE Trans. on Signal Processing, 2000, 48(8): 2195–2204.
[5] NEHORAI A, PALDI E. Vector-sensor array processing for electromagnetic source localization. IEEE Trans. on Signal Processing, 1994, 42(2): 376–398.
[6] YANG M L, DING J. A multiscale sparse array of spatially-spread electromagnetic-vector-sensors for direction finding and polarization estimation. IEEE Access, 2018, 6: 9807–9818.
[7] WU N, QU Z Y. Joint estimation of DOA and polarization based on phase difference analysis of electromagnetic vector sensor array. Multidimensional Systems & Signal Processing, 2018, 29(2): 597–620.
[8] CAO M Y, MAO X P. Tensor approach to DOA estimation of coherent signals with electromagnetic vector-sensor array. Sensors, 2018, 18(12): 4320.
[9] ZHENG G. Two-dimensional DOA estimation for polarization sensitive array consisted of spatially spread crossed-dipole. IEEE Sensors Journal, 2018, 18(12): 5014–5023.
[10] SONG H Y, YANG C Y. Vector-sensor array DOA estimation using spatial time-frequency distributions. Proc. of the IEEE International Conference on Consumer Electronics, 2018: 1−2.
[11] YANG M, DING J. Coprime L-shaped array connected by a triangular spatially-spread electromagnetic vector-sensor for two-dimensional direction of arrival estimation. IET Radar, Sonar & Navigation, 2019, 13(10): 1609–1615.
[12] AHMED T, ZHANG X F, WANG Z, et al. Rectangular array of electromagnetic vector sensors: tensor modelling/decomposition and DOA-polarisation estimation. IET Signal

Processing, 2019, 13(7): 689–699.
[13] SI W J, WANG Y, ZHANG C J. Three-parallel co-prime polarization sensitive array for 2-D DOA and polarization estimation via sparse representation. IEEE Access, 2019, 7: 15404–15413.
[14] SCHUTTE H D, WENZEL J. Hypercomplex numbers in digital signal processing. Proc. of the IEEE International Symposium on Circuits and Systems, 1990: 1557−1560.
[15] HAHN S L. Multidimensional complex signals with single orthant spectra. Proceedings of the IEEE, 1992, 80(8): 1287–1300.
[16] BULOW T, SOMMER G. Hypercomplex signals—a novel extension of the analytic signal to the multidimensional case. IEEE Trans. on Signal Processing, 2001, 49(11): 2844–2852.
[17] MIRON S, BIHAN N L. Quaternion-music for vector-sensor array processing. IEEE Trans. on Signal Processing, 2006, 54(4): 1218–1229.
[18] ZHAO J C, TAO H H. Estimation of DOA and polarization with COLD sensors based on quaternion model. Wuhan University Journal of Natural Sciences, 2017, 22(4): 361–368.
[19] ZHAO J C, TAO H H. Quaternion based joint DOA and polarization parameters estimation with stretched three-component electromagnetic vector sensor array. Journal of Systems Engineering and Electronics, 2017, 28(1): 1–9.
[20] ZHU Q, ZHENG G, PENG J Q. DOA estimation for electromagnetic vector-sensor array based on biquaternion. Proc. of the 3rd IEEE International Conference on Electronic Information and Communication Technology, 2020: 509−513.
[21] CHEN H, WANG W, LIU W. Augmented quaternion ESPRIT-type DOA estimation with a crossed-dipole array. IEEE Communications Letters, 2019, 24(3): 548–552.
[22] ROY R, KAILATH T. Esprit-estimation of signal parameters via rotational invariance techniques. IEEE Trans. on Acoustics, Speech, and Signal Processing, 1989, 37(7): 984–995.
[23] BOUDAHER E, AHMAD F. Mutual coupling effect and compensation in nonuniform arrays for direction-of-arrival estimation. Digital Signal Processing, 2017, 61: 3–14.
[24] PAL P, VAIDYANATHAN P P. Nested arrays: a novel approach to array processing with enhanced degrees of freedom. IEEE Trans. on Signal Processing, 2010, 58(8): 4167–4181.
[25] VAIDYANATHAN P P, PAL P. Sparse sensing with coprime samplers and arrays. IEEE Trans. on Signal Processing, 2010, 59(2): 573–586.
[26] YANG M L, SUN L. Improved nested array with hole-free DOA and more degrees of freedom. Electronics Letters, 2016, 52(25): 2068–2070.
[27] PAL P, VAIDYANATHAN P P. Coprime sampling and the music algorithm. Proc. of the Digital Signal Processing Workshop and IEEE Signal Processing Education Workshop, 2011: 289−294.
[28] QIN S, ZHANG Y D. Generalized coprime array configurations for direction-of-arrival estimation. IEEE Trans. on Signal Processing, 2015, 63(6): 1377–1390.
[29] ZHENG Z, WANG W Q. MISC array: a new sparse array design achieving increased degrees of freedom and reduced mutual coupling effect. IEEE Trans. on Signal Processing, 2019, 67(7): 1728–1741.
[30] KANTOR I L. Hypercomplex numbers: an elementary introduction to algebras. Berlin: Springer, 1989.
[31] WARD J P. Quaternions and cayley numbers: algebra and applications. Berlin: Springer Science & Business Media, 1997.
[32] LEE H C. Eigenvalues and canonical forms of matrices with quaternion coefficients. Proceedings. of the Royal Irish Academy, 1948, 52: 253–260.
[33] HOCTOR R T, KASSAM S A. The unifying role of the coarray in aperture synthesis for coherent and incoherent imaging. Proceedings. of the IEEE, 1990, 78(4): 735–752.
[34] LIU C L, VAIDYANATHAN P P. Super nested arrays: linear sparse arrays with reduced mutual coupling—part I: fundamentals. IEEE Trans. on Signal Processing, 2016, 64(15): 3997–4012.
[35] LIU J Y, ZHANG Y M. Augmented nested arrays with enhanced DOF and reduced mutual coupling. IEEE Trans. on Signal Processing, 2017, 65(21): 5549–5563.
[36] FRIEDLANDER B, WEISS A J. Direction finding in the presence of mutual coupling. IEEE Trans. on Antennas and Propagation, 1991, 39(3): 273–284.
[37] LIU C L, VAIDYANATHAN P P. Hourglass arrays and other novel 2-D sparse arrays with reduced mutual coupling. IEEE Trans. on Signal Processing, 2017, 65(13): 3369–3383.
[38] MUNIER J, DELISLE G Y. Spatial analysis using new properties of the cross-spectral matrix. IEEE Trans. on Signal Processing, 1991, 39(3): 746–749.
[39] LEO S D, SCOLARICI G. Quaternionic eigenvalue problem. Journal of Mathematical Physics, 2002, 43(11): 5815–5829.
[40] BIHAN N L, MARS J. Singular value decomposition of quaternion matrices: a new tool for vector-sensor signal processing. Signal Processing, 2008, 84(7): 1177–1199.
[41] BIHAN N L, SANGWINE S J. Quaternion principal component analysis of color images. Proc. of the International Conference on Image Processing, 2003: I-809.
[42] ZHANG F. Quaternions and matrices of quaternions. Linear Algebra and its Applications, 1997, 251(2): 21–57.
[43] WOOD R M W. Quaternionic eigenvalues. Bulletin of the London Mathematical Society, 1985, 17(2): 137–138.
[44] GERSTNER A B, BYERS R. A quaternion QR algorithm. Numerische Mathematik, 1989, 55(1): 83–95.

Biographies

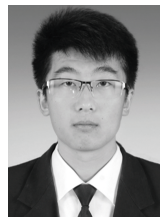

SHAO Shuai was born in 1993. He received his B.S and M.S. degrees in communication engineering and electronics and communication engineering from Harbin Institute of Technology, Weihai, in 2016 and 2018 respectively. He is currently working toward his Ph.D. degree in information and communication engineering at Harbin Institute of Technology. His past and present research involves high-frequency surface wave radar system array signal processing and signal time-frequency analysis and, more recently, polarization quaternion DOA estimation.
E-mail: 643218186@qq.com

LIU Aijun was born in 1971. He received his B.S and M.S. degrees in communication engineering and information and signal processing from Dalian Maritime University in 1995 and 2003 respectively, and his Ph.D. degree in information and communication engineering from Harbin Institute of Technology in 2011. He is an assistant professor at the School of Information and Electrical Engineering, Harbin Institute of Technology, Weihai. His research interests involve high-frequency surface wave radar system design and analysis, array signal processing, and signal time-frequency analysis.
E-mail: liuaijun@hit.edu.cn

YU Changjun was born in 1962. He received his B.S. degree in electronic engineering from Harbin Institute of Technology in 1984 and his M.S. and Ph.D. degrees in information and communication engineering from Harbin Engineering University in 1990 and 2010, respectively. He is a professor at the School of Information and Electrical Engineering, Harbin Institute of Technology, Weihai. His research interests involve high-frequency surface wave radar system design and analysis, target detection, estimation and tracing, and ionosphere remote sensing.
E-mail: yuchangjun@hit.edu.cn

ZHAO Quanrui was born in 1993. He received his B.S. degree in communication engineering and his M.S. degree in electronics and communication engineering from Harbin Institute of Technology in 2016 and 2020 respectively. He is a signal processing engineer in Shanghai Radio Equipment Research Institute. His research interests involve radar system design and analysis, array signal processing, and precision guidance.
E-mail: HIT_zhao@163.com